On the suitability of the $4^\circ \times 4^\circ$ GRACE mascon solutions for remote sensing Australian hydrology

Awange, J.L.[*,1,2], Fleming, K.M.[1], Kuhn, M.[1], Featherstone, W.E.[1], Heck, B.[2] and Anjasmara, I.[1]

[1] *Western Australian Centre for Geodesy and The Institute for Geoscience Research*
Curtin University
GPO Box U1987, Perth, Western Australia, 6845, Australia
[2] *Geodetic Institute*
Karlsruhe Institute of Technology
Engler-Strasse 7, D-76131, Karlsruhe, Germany
[*] *Corresponding author*
Phone: +61 (0) 8 9266 7600
E-mail: J.Awange@curtin.edu.au

Abstract

Hydrological monitoring is essential for meaningful water-management policies and actions, especially where water resources are scarce and/or dwindling, as is the case in Australia. In this paper, we investigate the regional $4^\circ \times 4^\circ$ mascon (mass concentration) GRACE solutions for Australia provided by GSFC (Goddard Space Flight Center, NASA) for their suitability in monitoring Australian hydrology, with a particular focus on the Murray-Darling Basin (MDB). Using principal component analysis (PCA) and multi-linear regression analysis (MLRA), the main components of spatial and temporal variability in the mascon solutions are analysed over the whole Australian continent and the MDB.

The results are compared to those from global solutions provided by CSR (Center for Space Research, University of Texas at Austin) and CNES/GRGS (Centre National d'Études Spatiales/Groupe de Recherche de Geodesie Spatiale, France) and validated using data from the Tropical Rainfall Measuring Mission (TRMM), water storage changes predicted by the WaterGap Global Hydrological Model (WGHM) and the Global Land Data Assimilation System (GLDAS), and ground-truth (river-gauge) observations. For the challenging Australian case with generally weak hydrological signals, the mascon solutions provide similar results to those from the global solutions, with the advantage of not requiring additional filtering (destriping and smoothing) as, for example, is necessary for the CSR solutions. A further advantage of the mascon solutions is that they offer a higher temporal resolution (i.e., 10 days) compared to approximately monthly CSR solutions. Examining equivalent water volume (EWV) time-series for the MDB shows a good cross-correlation (generally > 0.7) among the GRACE solutions when considering the whole basin, although lower (< 0.5) when all the GRACE solutions are compared to the TRMM, WGHM and GLDAS time-series. Examining smaller portions of the MDB see the correlation among the GRACE solutions and the TRMM, WGHM and GLDAS EWV time-series increase slightly (> 0.6), with all time-series appearing to visually follow the general behaviour of the river-

gauge data, although the cross-correlations are relatively low (between 0.3 to 0.6).
Keywords: GRACE, hydrology, mascons, Australia, water resources

---

1. Introduction

Climate change is one of the most challenging issues facing society today (Solomon et al., 2007), with Australia believed to be already feeling its impact (e.g., Nicholls, 2006). A major concern is the potential threat this poses to Australia's scarce freshwater resources. This point has become more pertinent given the recent drought that has afflicted many areas of Australia, the effects of which were possibly made worse by higher temperatures (e.g., Nicholls, 2004; Ummenhofer et al., 2009; Leblanc et al., 2009). There is thus a need for continuous information about the spatial and temporal variation of water resources to allow properly informed decisions by hydrologists and water-management authorities.

The GRACE (Gravity Recovery and Climate Experiment) space mission measures the spatial and temporal changes of the Earth's gravity field at regular time intervals (e.g., daily to monthly, Wahr et al., 1998; Tapley et al., 2004a,b). Such changes are the result of mass redistributions in the oceans (e.g., Wahr et al., 2002; Chambers et al., 2004), atmosphere (e.g., Swenson and Wahr, 2002; Boy and Chao, 2005), cryosphere (e.g., Velicogna, 2009; Baur et al., 2009), solid Earth due to processes such as glacial isostatic adjustment (e.g., Barletta et al., 2008; Tregoning et al., 2009) and, the subject of this work, terrestrial hydrology (e.g., Rodell and Famiglietti, 1999; Ramillien et al., 2004; Werth et al., 2009; Tiwari

et al., 2009). Observations from GRACE have offered a means of studying basin-scale water content variations at a precision potentially useful for hydrological studies and water-resource management (e.g., Syed et al., 2005; Crowley et al., 2006; Awange et al., 2008b; Chen et al., 2009; Klosko et al., 2009; Leblanc et al., 2009).

Within the context of Australian hydrology, Rodell and Famiglietti (1999) determined prior to the launch of GRACE (in 2002) that monthly, seasonal and annual changes in the total water storage of the Murray-Darling Basin (MDB) should be detectable by GRACE, a point reinforced by Ellett et al. (2006) who commented that GRACE would be suitable for such studies owing to the dominance of inter-annual groundwater variations. This was later verified by Leblanc et al. (2009) who, by combining GRACE and hydrological observations and modelling results, estimated a loss of groundwater from the MDB of $\sim$ 104 km^3 between 2001 and 2007. Chen et al. (2005) derived GRACE-based estimates of terrestrial water storage variability for the Victoria Basin, Northern Australia, finding good agreement with values provided by the Global Land Data Assimilation System (GLDAS, Rodell et al., 2004).

Although the foregoing discussion highlights the potential of GRACE to monitor Australia's freshwater resources, Awange et al. (2008a, 2009) found that when

using standard global (spherical harmonic) solutions commonly employed for larger basins such as the Amazon (e.g., Wahr et al., 1998; Tapley et al., 2004a,b), there are several factors that limit the usefulness of GRACE gravity field solutions for Australian hydrological studies. These are: 1) The relatively small hydrological signal that is experienced over much of Australia (with the exception of the tropical north), which is diminished further by the recent, and in some areas ongoing, drought. Such a low signal is very difficult to detect using the current GRACE system and processing strategies. 2) The effect of the occurrence of considerable spatial and spectral leakage from the surrounding oceans that masks potential terrestrial hydrological signals detectable by GRACE.

In order to provide meaningful water-management policies and actions over higher spatial (smaller basins) and temporal (less than one month) scales, Awange et al. (2009) proposed two avenues that could be explored to better exploit GRACE results for Australian water storage studies: 1) The use of more regional solutions such as those arising from mass concentration (mascon) methods (e.g., Lemoine et al., 2007a), wavelets (e.g., Fengler et al., 2007), or regional inversion (e.g., Han et al., 2005), rather than the global spherical harmonic approach. 2) The use of post-processing filtering techniques that are better suited to the Australian situation. For example, regarding the global spherical harmonic solutions, Lemoine

et al. (2007a) point out that errors in the dynamic models used in these solutions that occur in one part of the globe corrupt the time-variable gravity field recovered elsewhere, an observation also noted by Brown and Tregoning (2010). This is because spherical harmonics are globally supported basis functions (e.g., Blais and Provins, 2002). Therefore, Lemoine et al. (2007a) propose the use of the mascon approach (Muller and Sjogren, 1968) to alleviate such problems.

The aim of this study is to investigate the suitability of one of the regional solution products, namely the $4^\circ \times 4^\circ$ mascon solutions for Australia of NASA's Goddard Space Flight Center (GSFC, Lemoine et al., 2007a), for monitoring Australian hydrology over continental and smaller spatial scales, in particular more localised areas such as the MDB. Comparisons are made with two other GRACE solutions: the RL04 release provided by the Center for Space Research (CSR), University of Texas at Austin (Bettadpur, 2007), and the second release from the Centre National D'Études Spatiales/Groupe de Recherche de Geodesie Spatiale, France (CNES/GRGS, Lemoine et al., 2007b; Bruinsma et al., 2010). In addition, these results are compared to rainfall measurements over Australia as obtained from the Tropical Rainfall Measuring Mission (TRMM, Kummerow et al., 1998, 2000), water storage values predicted by the WaterGap Global Hydrological Model (WGHM, Döll et al., 2003) and the Global Land Data Assimilation

System (GLDAS, Rodell et al., 2004), and ground-truth information in the form of river-gauge data.

It should be pointed out that precipitation plays an important role in the terrestrial water balance, being the replenishment source of large-scale water storage. According to the terrestrial water balance, precipitation is equal to the sum of evapotranspiration, runoff and water storage changes (e.g., Davie, 2008). Therefore, it is important to emphasize that when interpreting the results in this work, there is no one-to-one relation between water storage and precipitation, as the former also changes due to evapotranspiration and runoff. However, analysing precipitation and water storage provides information on their overall relationship, as well as indirect information on the combined effect of evapotranspiration and runoff, by closing the water budget (e.g., Davie, 2008). A recent study by Rieser et al. (2010), for instance, revealed a direct relationship between the GRACE and TRMM data sets over most parts of Australia, where the GRACE-derived surface mass changes were found to exhibit smoother spatial and temporal variations and were better suited to detecting long-term trends in the presence of strong annual signals, which can adversely affect long-term trend estimates.

The spatial and temporal trends in the different data sets are assessed using principal component analysis (PCA) and multi-linear regression analysis (MLRA).

In addition, cross-correlation analysis is applied to the PCA and MLRA results to assess the strength of the relationship among the datasets investigated.

2. Datasets

2.1. GRACE solutions

Background to the GRACE mission: GRACE (launched 17th March 2002) is a joint United States/German space mission dedicated to monitoring temporal and spatial variations of the Earth's gravity field on a global scale. It employs two low-Earth orbiting satellites in the same orbital plane ($\sim$ 460 km altitude, $\sim 89.5^{\circ}$ inclination) operating in tandem (i.e., one following the other at $\sim$ 220 km distance) (Wahr et al., 1998; Tapley et al., 2004a,b). The separation of the satellites is measured by a K-band range rate system (KBRR) and orbits are obtained using data provided by a GPS receiver and satellite laser ranging reflectors on board the spacecraft. Other information, such as that provided by on-board accelerometers, are used to correct for non-gravitational effects such as atmospheric drag and solar radiation pressure (e.g., Milani et al., 1987). Gravity field solutions that describe the spatial and temporal changes in the Earth's gravity field are generated at regular intervals (e.g., daily to monthly) by several institutions worldwide. Each institution makes use of different forward models to accommodate tides, atmospheric and oceanic dynamics etc., therefore some difference in the final solutions should be expected.

Mascon solutions: The main goal of the $4^{\circ} \times 4^{\circ}$ mascon approach is to recover

sub-monthly mass flux at a higher spatial resolution (160,000 km^2, cf. 400,000 km^2 for CSR; Swenson et al., 2003; Rowlands et al., 2005) from GRACE in order to provide estimates of the entire hydrological signal (Rowlands et al., 2005, 2010; Luthcke et al., 2006; Lemoine et al., 2007a). Advantages of the mascon approach over standard spherical harmonic solutions (see e.g., Rowlands et al., 2010) include the minimisation of leakage, easier application of spatial constraints, and higher spatial and temporal resolution (see below).

The mascon solutions provided by GSFC are inferred from KBRR data without incorporating GPS data (Rowlands et al., 2005; Han et al., 2005; Lemoine et al., 2007a), unlike the global solutions used in the CNES/GRCS or CSR releases. The reason for the omission of the GPS data is that the GPS-related errors are much greater than those in the KBRR. GSFC is also in the process of producing global equal-area 2° mascon solutions, details of which have been published, e.g., in Rowlands et al. (2010), although they have yet to be released to the public for use and analysis. There are also mascon-type solutions in the process of being generated by the Jet Propulsion Laboratory (JPL, Mike Watkins, 2010, *pers. com.*), which do take into consideration the GPS observations, but have also not yet been released to the public.

The application of the GSFC mascon method for Australia requires the divi-

sion of continental regions into $4^\circ \times 4^\circ$ blocks. The change in mass over each block is then estimated in terms of equivalent water thickness (EWT) for every 10 days. Whereas various filters (e.g., smoothing and destriping) are usually required to smooth the gravity solutions described by the spherical harmonic coefficients provided by CSR, the mascon method smooths the solutions by combining spatial and temporal constraint equations together with GRACE KBRR tracking data in a simultaneous least-squares solution.

The formulation for the mascon approach makes use of the fact that a change in potential caused by adding a small uniform layer of mass over a region at an epoch, t, can be represented as a set of (differential) potential coefficients that can be added to a mean background field. The differential coefficients are computed for each $4^\circ \times 4^\circ$ mascon as (Lemoine et al., 2007a):

$$\Delta A_{lm} = \frac{(1+k_l')R^2\sigma(t)}{(2l+1)M} \int Y_{lm}(\Omega) d\Omega, \tag{1}$$

where l and m are the spherical harmonic degree and order, respectively, k_l is the loading Love number of degree l, R and M are the mean radius and mass of the Earth, respectively, Ω is a representation of the surface area, Y_{lm} is the spherical harmonic of degree and order l and m corresponding to the potential coefficient A_{lm}, and $\sigma(t)$ is the mass of the layer over a unit of surface area $\Delta\Omega$ at epoch t.

Spatial and temporal constraints are then applied to ensure neighbouring mascons stay close to each other in value (Rowlands et al., 2005), the weighting applied being a function of the mascons' relationship in time and space, given by

$$\exp[2 - \frac{d_{ij}}{D} - \frac{|t_{ij}|}{T}]. \quad (2)$$

In Eqn. (2), T and D are the correlation time and distance, respectively, employed to form the constraint, d_{ij} is the distance between mascons i and j, and t_{ij} is the difference in time tags for mascons i and j. From Eqns. 1 and 2, EWT values for each $4^\circ \times 4^\circ$ mascon are computed. In addition, since these solutions are regional, KBRR data from a buffer zone of 8° surrounding Australia are included when generating the mascon solutions. No KBRR data is used from outside this buffer zone, which also helps to reduce leakage (Frank Lemoine, 2010, *pers. com.*). More details about the mascon method can be found e.g., in Muller and Sjogren (1968); Rowlands et al. (2005); Lemoine et al. (2007a); Rowlands et al. (2010). The 10-day average EWT values over a $4^\circ \times 4^\circ$ grid for continental regions from April 2003 to April 2007 are provided online (see the Acknowledgements).

CSR solutions: These global spherical harmonic solutions are amongst the more commonly used of the GRACE releases (Bettadpur, 2007) and are provided as fully normalised spherical harmonic coefficients of the geopotential up to de-

gree and order 60, since coefficients at higher degrees are too strongly affected by noise. In this study, the release RL04 standard monthly GRACE solutions provided by CSR (currently available from 04.2002 to 07.2010) are used to generate EWT values for Australia using the approach of Wahr et al. (1998), with respect to a static field model (GGMO2S, Tapley et al., 2005). The correlated-error filter proposed by Swenson and Wahr (2006) to reduce the north-south striping and a Gaussian filter of radius 500 km (e.g., Wahr et al., 1998) to remove high-frequency errors were applied prior to the synthesis of the spherical harmonic coefficients to the spatial domain. These striping and high-frequency effects potentially mask hydrological signals over Australia, making their detection extremely difficult (cf. Awange et al., 2008b).

CNES/GRGS solutions: These are also global solutions, providing $1^\circ \times 1^\circ$ grids of EWT taken with respect to a satellite-only reference field (EIGEN-GRGS.RL02.mean-field; Bruinsma et al., 2010). They have a 10-day temporal resolution, with the actual solutions processed to spherical harmonic degree and order 50 (e.g., Lemoine et al., 2007b; Bruinsma et al., 2010). These solutions have been chosen as part of this work because they have the same temporal resolution (i.e., 10 days) as the mascon solutions. The processing of the solutions makes use of the GRACE KBRR and GPS data, as well as data from LAGEOS-1/2 SLR measurements.

The coefficients are constrained individually to the above-mentioned reference field (see Eqn. 1, Bruinsma et al., 2010), leading to these solutions not requiring additional post-processing filtering such as destriping or Gaussian filtering, as is the case for the CSR solutions (Bruinsma et al., 2010).

2.2. Tropical Rainfall Measuring Mission (TRMM) 3B43 product

TRMM is a joint mission between the United States (NASA) and Japan (Japan Aerospace Exploration Agency) (Kummerow et al., 1998, 2000; Huffman et al., 2007). TRMM orbits at an altitude of $\sim$ 403 km with an inclination of 35°, and has an orbital period of about 91 minutes, thus completing about 16 revolutions per day. TRMM was designed to monitor and study tropical rainfall in the latitude range $\pm 50^{\circ}$ over inaccessible areas such as the oceans and un-sampled terrains. The primary instruments are the TRMM Microwave Imager (TMI), the Precipitation Radar (PR) and the Visible and Infrared Radiometer System (VIRS) (Kummerow et al., 1998).

The product used in this work (3B43) is a monthly global average derived from the TRMM instruments, as well as data from a number of other satellites and ground-based rain-gauge data (Kummerow et al., 2000; Huffman et al., 2007). The data is provided as mm hr^{-1} EWT, which we convert to mm EWT for each month by simply multiplying the original value by the number of hours in a given

month. TRMM products have been used in several studies in conjunction with the GRACE solutions to examine water storage changes and to attempt to close the terrestrial water budget (e.g., Crowley et al., 2006; Rieser et al., 2010).

2.3. Terrestrial water storage models

The WaterGap Global Hydrological Model (WGHM, e.g., Döll et al., 2003; Güntner et al., 2007) is the global hydrological part of the WaterGAP (Water-Global Assessment and Prognosis) global model of water availability and use. WGHM is provided as EWT on a $0.5^\circ \times 0.5^\circ$ grid and covers the global land area with the exceptions of Greenland and Antarctica. It represents the major hydrological components, namely rainfall, snow accumulation and melting, evapotranspiration, runoff, and the lateral transport of water within river networks. It considers soil moisture within the effective root zone of vegetated areas, water storage on the vegetation canopy, groundwater (namely recharge and depletion by outflow into river systems), and surface water in the form of rivers, natural lakes, wetlands and man-made reservoirs. Details of the model may be found in Döll et al. (2003) and Güntner et al. (2007).

The Global Land Data Assimilation System (GLDAS, e.g., Rodell et al., 2004) has been developed to generate various fields that describe the state of the land surface in terms of terrestrial energy and water storage and flux. It makes

use of ground- and space-based observations (e.g., TRMM being input for the precipitation component) that are incorporated into land surface models, of which there are three: Mosaic, Noah and the Community land Model. Of these, the time series used in this work comes from Noah (Ek et al., 2003; Rodell et al., 2004). A major difference between GLDAS and WGHM is that GLDAS does not accommodate ground or surface water changes, both of which are important components of terrestrial water storage (see e.g., Syed et al., 2008).

2.4. In-situ data

The sets of in-situ data used in this study consist of river-gauge data, providing heights of the water level at four stations along the Murray River within the MDB. The location of these solutions (see Figure 5) are Yarrawonga, Swan Hill, Euston and Torrumbarry. The data are provided by the Murray-Darling Basin Authority (see the Acknowledgements). Although the presence of dams and reservoirs along the river would significantly affect flow, the aim of this part of the study is to see if a general correlation, over seasonal scales, between river flow and the GRACE observations could be found.

2.5. Data preparation

In order to maintain some consistency when comparing and analysing the results for each dataset, the following were applied to each time series.

- All datasets were converted to the same $0.25^\circ \times 0.25^\circ$ grid, making use of routines of the Generic Mapping Tools suite of programs (Wessel and Smith, 1998), specifically, `triangulate` (performs Delaunay triangulation to determine how the grid points are connected to give the most equilateral triangulation possible), `surface` (fits an adjustable continuous curvature surface) and `grd2xyz` (converts a gridded file to its equivalent table with location and values). Details may be found on the GMT website (http://gmt.soest.hawaii.edu). The reason for this is to allow the spatial cross correlations in the results between datasets to be carried out (see below), with $0.25^\circ \times 0.25^\circ$ being the grid of the TRMM dataset.

- Since the CSR GRACE solutions are filtered using a Gaussian filter of radius 500 km (see, e.g., Baur et al., 2009) for reasons already stated in Sect. 2.1, a Gaussian filter of radius 500 km was also applied to the TRMM, GLDAS and WGHM datasets to remove the higher-frequency signal and enable them to be more easily compared to the CSR GRACE solutions.

- All datasets were masked to remove signals from outside Australia (i.e., the values outside Australia were set to zero).

3. Methods

To compare the mascon solutions to the global spherical harmonic solutions with respect to Australia's spatial and temporal variations of stored water from 04.2003 to 04.2007 (the period covered by the mascon solutions used in this work) two statistical approaches are used, i.e., principal component analysis (PCA, e.g., Preisendorfer, 1988) and multi-linear regression analysis (MLRA, e.g., Montgomery and Peck, 1992). These methods are chosen owing to their suitability to separate out the spatial and temporal behaviour of complex systems (as demonstrated in e.g., Rieser et al., 2010). To examine how the different GRACE solutions, TRMM rainfall and the GLDAS and WGHM hydrological models relate to each other, the cross-correlations between the different datasets of the results arising from the MLRA are determined. A visual comparison is also made to assess the relative susceptibility of the different GRACE solutions to the north-south striping.

Principal Component Analysis (PCA): PCA is a statistical method and when applied to spatio-temporal data sets (as done in this study) can be used to identify the most dominant spatial and temporal variability (e.g., Preisendorfer, 1988). The PCA decomposes the spatio-temporal data set (reduced by the long-term average) into sets (modes) of empirical orthogonal functions (EOFs) and principal com-

ponents (PCs) corresponding to the spatial and temporal variations, respectively. When ordered with respect to their relative importance, most of the variability is usually contained in the first few modes, therefore making it possible to significantly reduce the complexity of the original data set, while retaining the most dominant variability.

It needs to be emphasised that there is no need for the PCA to differentiate between the physical origins of the various signals, since it is a purely statistical method and so does not only analyse particular signals. The strength, however, of PCA is that it reveals the most dominant spatial and temporal variations that usually describe a large part of a signal's overall variability. As will be shown, in our case, the PCA reveals that a linear trend and annual signal explains a large part of each of the time series' variability over most parts of Australia by the information present in modes 1 and 2.

Multi-linear regression analysis (MLRA): MLRA involves examining the temporal and spatial behaviour of a dataset using a simple time-variable model. For the GRACE time series, the model used in this work is given by

$$y(t_i) = A + Bt_i + Csin(\omega_a t_i) + Dcos(\omega_a t_i) + Esin(\omega_{S2} t_i) + Fcos(\omega_{S2} t_i), \quad (3)$$

where A is an offset, B is the linear trend, ω_a and ω_{S2} denote the annual fre-

quencies of the annual and S2 tidal (161 days) aliasing signals, respectively, and C, D, E and F represent the inferred annual and S2 tidal terms, respectively. The S2 tidal aliasing term is the combined result of the miss-modelling of the oceanic and atmospheric tides and sampling with the GRACE repeat orbit (see e.g., Melachroinoa et al., 2009). For the other time series (i.e., TRMM, GLDAS and WGHM), we use the same equation, except we exclude the S2 tidal aliasing term as it is not relevant to these datasets. While using a simple linear trend and sinusoial model is in some ways simplistic given interannual variations would make the annual variations not a pure 1 year signal, Rieser et al. (2010) showed that statistically, over most of Australia, a functional model that includes a linear trend and annual signal is significant. They also noted that no statistical improvement in the model fit is achieved when adding further periodic signals like a semi-annual signal. As all the time series are provided over different time periods, we employ the period covered by the mascon solutions, i.e., 4 complete years, to reduce the bias in the inferred trends that may arise from different time spans.

Cross-correlation analysis: Cross-correlations are carried out in time and space to examine how the results from the MLRA compare between any two datasets. This is given by

$$R = \frac{\sum_{i=1}^{n}[(x(i) - \bar{x})(y(i) - \bar{y})]}{\sqrt{\sum_{i=1}^{n}(x(i) - \bar{x})^2}\sqrt{\sum_{i=1}^{n}(y(i) - \bar{y})^2}}, \quad (4)$$

where x and y are the datasets under consideration, $\bar{x}$ and $\bar{y}$ their respective means, and n is the number of data (i.e., the number of grid points or data within a time-series). This is applied to the linear and annual terms and the annual phase relations inferred from Eqn. 3 for each of the datasets examined (see Table 1) as well as between the datasets and ground-truth data (see Table 2).

Localised assessments: When we examine the temporal variability in the GRACE solutions, TRMM rainfall, and GLDAS and WGHM hydrological models over more localised scales, that is the MDB and subsections within it (see Figure 5), we first determine, for each dataset time-series, the equivalent water volume (EWV) associated with each area. This is done by summing the product of the area of each grid cell that makes up the area of interest and multiplying by the associated EWT. Once the EWV has been found, a moving average filter equivalent to three months is applied to each EWV time-series. This enables us to examine the seasonal variability in the time-series, without the presence of shorter-term variations (e.g., monthly). Similarly, we apply this temporal filter to the in-situ data (river-gauge). Although the in-situ data represents a specific point, we take the average of several

river-gauge time-series to gain an average for a given $4^\circ \times 4^\circ$ element. The aim of this comparison is to determine if, for the case of Australia, the $4^\circ \times 4^\circ$ mascon solutions are representative of smaller areas.

4. Results and analysis

4.1. Australia-wide case

Figure 1 presents the EWT values of each GRACE release studied for each month of 2005, where for the mascon and CNES/GRGS solutions, the average for the three corresponding 10-day solutions are used. We also determine the cross correlation (Eqn. 4) between the mascon (Figure 1a) and CSR (Figure 1b) and mascon and CNES/GRGS (Figure 1c) solutions for each month, the resulting values being included in Figure 1b,c. In general, cross correlation values associated with the CSR and CNES/GRGS solutions follow a similar pattern in terms of which months display the higher R values and which the lower, i.e., the winter months appearing to show lower values than summer, especially so for CSR. Based on these values for this year, the mascon solutions appear to match the CSR solutions better for a greater proportion of the year.

Whereas the results of CNES/GRGS from Figure 1c are seen to be significantly affected by the north-south stripes, this is not seen in the mascon (Figure 1a) and to a lesser extent in the CSR solutions. The mascon approach imposes the restriction that only the data within a 8° buffer zone (see discussion in Sec. 2.1) are used in order to reduce leakage. However, since uniform constraints are applied for the equal-angle $4^\circ \times 4^\circ$ mascon solutions, it is possible that there is still

some leakage. This effect is addressed in the future 2° mascon release where separate constraints are applied to each area (Rowlands et al., 2010). The destriping filtering (see Sect. 2.1) carried out on the CSR solutions has the disadvantage that some small hydrological signals could be erroneously filtered out. The mascon solutions therefore offer the advantage that the publicly available solutions can be used adequately without the user worrying about additional processing.

[FIGURE 1]

For the PCA, we first look at the Australia-wide case, mainly to compare the different GRACE releases among themselves and with the TRMM, GLDAS and WGHM time-series. The results of the PCA analysis for modes 1 and 2 are shown in Figures 2 and 3, respectively. We note that most of the variability is contained in the first mode (generally $> 60\%$), while considering the first 2 modes together accommodates between *ca.* 76% (for TRMM) and *ca.* 87% (for CSR) of the total variability of each signal.

[FIGURE 2]

[FIGURE 3]

The 1st mode (Figure 2) shows similar behaviour among all datasets, with all data displaying a general north-south varying EOF pattern and strong annual signal in the PC, indicative of seasonal variations. The annual signal is also apparent

in the mascon 2nd PC mode (Figure 3), but less so in the other datasets.

The dominant signal in northern Australia is a result of the annual monsoonal rains, and is much stronger than that from the southern part of the continent. Therefore, the 1st mode is dominated by changes in the north which may lead to smaller hydrological changes in the south being excluded from this mode. The northern signal is very obvious in the 1st mode EOF patterns for all datasets examined, and also in the 2nd mode EOF for the mascon, CNES/GRGS, CSR, TRMM and GLDAS time-series. The PC of the 2nd mode also appears to show strong linear trends in the time-series, especially for the CNES/GRGS, CSR and GLDAS results. For both the 1st and 2nd modes, central Australia shows a relatively low signal, a consequence of the small hydrological changes that are a result of the aridity of this area, although the signal that is present appears to indicate a mass loss. The shift in seasons with the higher rainfall (summer in the north, winter in the south) can be seen by the opposite signs in the signals given by the EOF, especially noticeable in Figure 2. All examined GRACE solutions are therefore capable of delivering the same information when considering the 1st mode, but when considering the 2nd mode, only the mascon identifies clearly an annual signal. This, however, is due to the higher proportion of signal in this mode for mascon (35%) compared to the others, who had a greater proportion of their signal

in the 1st mode.

The results of fitting a constant trend and seasonal signal described in Eqn. 3 are shown in Figure 4. The first point to note is that the linear trends resulting from the CNES/GRGS time-series (Figure 4b) appear to be larger in magnitude when compared to the others, although they are closer, at least in their spatial pattern, to CSR. What is apparent from the plots of the linear trends (Figure 4a–f) is a loss of mass (or decrease in rainfall) in the southeast as revealed by all datasets, a gain in the north, and a mixture in the southwest, where the mascon, TRMM, GLDAS and WGHM time-series show a loss while the CNES/GRGS and CSR exhibit a gain, although there is a major area of loss further inland for the CNES/GRGS. Note also how the TRMM and GLDAS appear closer to each other than to WGHM, remembering that TRMM is one of the input datasets for GLDAS. The magnitudes of the annual term (Figures 4g–l) appear very strong, as one would expect, in the north of the continent, with much lower amplitudes in the central regions for the CNES/GRGS, TRMM, GLDAS and WGHM datasets, which is expected given this region's aridity. The phase of the annual signal (Figures 4m–r) show the north-south variation where the monsoonal rains occur in the summer months/early in the year, while the southeast experiences wetter autumns. Again, similarly to what was seen in the PCA results, the dominance of the annual signal, as well as that

from northern Australia, is apparent. Here again, each GRACE solution appears to show the same capability without any outperforming the others.

[FIGURE 4]

[TABLE 1]

Next we present the cross-correlation (Eqn. 4) between dataset pairs of the inferred linear trends, annual amplitudes and phases in Table 1. The similarity observed between the annual terms is confirmed by the much higher values of the cross-correlation between datasets (generally > 0.8 for amplitude and > 0.7 for phase), while the linear terms show relatively low correlations (generally < 0.5), in particular when one compares CSR and the TRMM (0.19), although all of the GRACE solutions display a very low correlation with the TRMM and WGHM (generally < 0.5), which in turn show little correlation with each other, although the GRACE datasets display a slightly higher correlation with GLDAS (between 0.50 and 058). Note also that while the annual amplitude and phase correlate quite well between GLDAS and WGHM (0.91 and 0.72, respectively), the linear trend is rather poor (0.48). This should be expected as these models do not consider the same components of water storage, i.e., GLDAS neglects surface and ground water.

Comparing the PCA (Figures 2 and 3) and MLRA (Figure 4) results, the first

point to be made is how the 1st PCA mode appears to represent the temporal models' annual term (compare Figure 2 with the annual amplitudes in Figure 4), in both cases reflecting how the changes are dominated by the strong signal in the north. On the other hand, the 2nd PCA mode (Figure 3) in general is more difficult to interpret given its noisier nature, evident by the much lower percentage of contribution to the total variability, with the exception of the mascon. Considering also the temporal change terms inferred using Eqn. 3, both forms of analysis show seasonal changes to be the dominant feature of variation in mass (gravity field time-series), rainfall and water storage, which is furthermore dominated by the northern Australian signal. What is also shown in both analyses is an apparent gain in mass or water in the north, and a loss of mass is identified in the south east of the continent, particularly in the MDB.

The Australia-wide results therefore indicate that the $4^\circ \times 4^\circ$ mascon solutions do not provide any real advantage over the global solutions (CSR and CNES/GRGS). However, it has the advantage of not requiring the destriping and filtering processes as needed by the CSR, nor is the striping actually apparent, as is for the case of the CNES/GRGS.

4.2. Application to the Murray-Darling Basin (MDB)

We now turn our attention to the MDB to determine if the mascon method is superior to the other GRACE solutions for more localised areas, since the MDB is one of Australia's most important regions for agricultural production and is an area that has been severely affected by the recent drought conditions (Ummenhofer et al., 2009; Leblanc et al., 2009). We first examine the area outlined in Figure 5 denoted as A, which is defined by the mascon grid elements that cover much of the MDB. Figure 6 compares the inferred EWV variation from each dataset. As mentioned in section 3, we apply a moving average filter equivalent to three months to each time-series to remove the higher-frequency variations. The values are normalised to their respective averages to allow them to be more easily compared.

[Figure 5]

Examining first the three GRACE solutions in Figure 6 over the time period covered by the mascon solutions (grey shaded area), we note that the time-series generally follow each other reasonably well, as also shown by the resulting cross correlation values (Table 2), although CNES/GRGS shows greater variability than the others. From the cross-correlation values, CSR and CNES/GRGS, being global solutions, appear to be in closer agreement with each other ($R = 0.83$),

than when compared to the mascon (mascon to CNES/GRGS, $R = 0.70$, and mascon to CSR, $R = 0.75$). However, the correlations are much lower when the GRACE solutions are compared to the TRMM and WGHM time-series (< 0.5), similar to what was seen in the Australia-wide case.

Applying Eqn. 3 to these time-series for the period covered by the mascon solutions reveals a rate of change in EWV of -10.6 km^3/year for the mascon, -11.3 km^3/year for the CSR, but -28.9 km^3/year for the CNES/GRGS. The higher value for the latter is to be expected given that the CNES/GRGS rates were much greater than those from the mascon or CSR (see Figure 4). On the other hand, TRMM shows a rate of change in precipitation equivalent to -6.0 km^3/year, GLDAS -7.7 km^3/year, while for WGHM, a much lower rate of -1.9 km^3/year is found. What is also apparent from Figure 6 is the negative trend in the time-series of the GRACE solutions during the study period (2003-2007), which, however, appears to reverse just towards the end of 2007, in line with greater rainfall which is also reflected by WGHM, although CNES/GRGS appears to fit rather well the GLDAS (0.81).

[FIGURE 6]

[Table 2]

Examining the MDB in more detail, Figure 7 shows a similar plot as Figure 6, but for the sectors denoted in Figure 5 as B and C, as well as the combined B and

C sectors, which we denote as BC, and the river-gauge data whose locations are shown in Figure 5 (also smoothed with the three month moving average filter). We also determine the cross-correlation (Table 2) among the solutions and datasets. In Figure 7, we have removed from each time-series its average to simplify the comparison between datasets. For each of the two individual sectors (Figures 7a and b), there is a general agreement amongst the GRACE, TRMM, GLDAS and WGHM time-series, although a general pattern with respect to differences cannot be identified. When we compare these time series with the ground-truth data, visually, there appears to be a general correspondence between them. This correspondence in turn improves when these individual areas are combined, i.e., sector BC (Figure 7c).

However, the actual cross-correlation values are rather low, between 0.21 and 0.36 for the mascon-river-gauge data comparison, although better for the CNES/GRGS-river-gauge comparison (between 0.41 to 0.59). For these smaller areas (i.e., sectors B, C, and BC in Figure 5), the correlation values as seen from Table 2 are higher between the GRACE, TRMM, GLDAS and WGHM datasets, especially so when considering the TRMM, GLDAS and WGHM time-series (generally $>$0.8). We also note that the CSR and CNES/GRGS solutions show a higher correlation with each other than with the mascon solution.

[FIGURE 7]

As with the Australia-wide results, for the localised MDB, little advantage was noticed in the use of the $4^\circ \times 4^\circ$ mascon solutions over the filtered global solutions, although the rates of change inferred for the CSR and mascon solutions were closer to each other than those found from CNES/GRGS (see Table 2). Comparing the EWV changes with the river-gauge observations, all examined GRACE time-series followed the general pattern of the river-gauge data. For localised Australian cases, e.g., the MDB, the mascon method fails to offer an outright advantage over the global solutions, as was the case in the Australia-wide results.

5. Conclusions

This work set out to assess the potential for the mascon time-series of GRACE gravity field solutions to better serve Australian hydrological studies than global spherical harmonic releases. We found that:

1. Looking at Australia as a whole, compared with the examined global solutions (CSR and CNES/GRGS), the mascon solutions do not appear to provide significantly more information. We must, however, emphasise that Australia is a difficult test case, with a very low hydrological signal, made worse by the drought that has afflicted many parts of the country during the study period. Nonetheless, mascons are still able to identify the major climatological features of Australia, namely the dominance of the monsoonal rainfall over northern Australia, and the approximately six month offset between the wet seasons in the north and south of the continent, as well as identifying areas of mass gain (northern Australia) and mass loss (southern Australia).
2. Examining smaller scale regions such as the MDB, there again appears to be little advantage in the use of mascon solutions over the global solutions, although again the rates of change inferred for the CSR and mascon solutions are more closely related than those from CNES/GRGS. Comparing

the results with ground-truth data show all GRACE time-series follow the general pattern of the river-gauge data, although with a fairly low cross correlation, with CNES/GRGS showing a slightly stronger correlation (see Table 2). The lower correlations may be the result of anthropogenic regulation of river flow.

3. The overriding advantage of the $4^\circ \times 4^\circ$ mascon solutions for monitoring Australia's hydrology, however, is seen in the fact that its readily available solutions do not need post-processing filtering to remove the effects of leakage and the north-south stripes as required for the global spherical harmonic solutions (CSR), while some remnant striping remains in the CNES/GRGS solutions. Although leakage may still occur, the fact that the mascon solutions are comparable to post-processed global solutions is commendable.

Mascon also offers high temporal resolutions (10 days) compared to the CSR global solutions (30 days). Although the CNES/GRGS approach also offer 10 days solutions, they are affected more by the north-south stripes (Figure 1), thereby possibly making the mascon method the better option.

From this study, we therefore propose that, given the advantages of not requiring additional filtering and the 10-day temporal resolution, the mascon solutions are the preferred choice. However, this is only valid when one is interested in

the time period covered by the mascon time series, as they were only produced from April, 2003 until April, 2007. On the other hand, the CSR and CNES/GRGS solutions are still being generated, and of these two, the destriped and filtered CSR are the preferred, since the CNES/GRGS appear more affected by the north-south striping, and the resulting temporal change parameters differ greatly from the other examined GRACE solutions. In fact, the requirement of additional processing (destriping and filtering) for the CSR solutions allows a greater degree of freedom for users who prefer to deal directly with the provided spherical harmonic solutions.

Whereas the mascon solutions investigated in this study are derived from regional solutions on an equal-angle $4^\circ \times 4^\circ$ grid that uses uniform constraints, there will be a future 2° mascon release with separate constraints between time and space applied for different regions (Rowlands et al., 2010). Therefore, when it becomes available, the 2° mascon release will be assessed to determine if it is more beneficial to Australian hydrological studies than its $4^\circ \times 4^\circ$ predecessor.

Acknowledgments

The authors are grateful to F. Lemoine GSFC and the three reviewers whose comments and suggestions have significantly improved the manuscript. This research was supported under the Australian Research Council *Discovery Projects* funding scheme (project number DP087738). J.L. Awange acknowledges the financial support of a Curtin Research Fellowship and the Alexander von Humboldt (Ludwig Leichhardt Memorial Fellowship) Foundation that support his time at Curtin University and Karlsruhe Institute of Technology, respectively. M. Kuhn acknowledges the support of a Curtin Research Fellowship. I. Anjasmara acknowledges the support of The Institute for Geoscience Research (TiGeR). W. Featherstone is the recipient of an Australian Research Council Professorial Fellowship (project number DP0663020). The authors further wish to thank A. Güntner of GFZ Potsdam for making WGHM available, O. Baur of the Space Research Institute (Austrian Academy of Sciences) in Graz for providing his post-processed CSR solutions and E. Forootan of the University of Bonn for the reformatted GLDAS time series. The authors are also grateful for the other datasets used in this work, which may be obtained from the following sources:

- mascon NASA Access Program (http://grace.sgt-inc.com/index.html).
- CNES/GRGS GRACE solutions (http://bgi.cnes.fr:8110/geoid-variations/README.html).

- TRMM, Goddard Earth Sciences Data and Information Services Center (http://disc.sci.gsfc.nasa.gov/precipitation).
- The Murray-Darling Basin Authority (http://www.mdba.gov.au).
- Australian drainage divisions and river basin boundaries, Bureau of Meteorology (http://www.bom.gov.au/hydro/wr/basins).

This work is a TIGeR (The Institute of Geoscience Research) publication (no. 238).

References

Awange, J., Sharifi, M., Baur, O., Keller, W., Featherstone, W., Kuhn, M., 2009. GRACE hydrological monitoring of Australia: current limitations and future prospects. Journal of Spatial Science 54 (1), 23–36.

Awange, J., Sharifi, M., Keller, W., Kuhn, M., 2008a. GRACE application to the receding Lake Victoria water level and Australian drought. In: Sideris, M. (Ed.), Observing our Changing Earth. Springer, Berlin, pp. 387–396.

Awange, J., Sharifi, M., Ogonda, G., Wickert, J., Grafarend, E., Omulo, M., 2008b. The falling Lake Victoria water level: GRACE, TRIMM and CHAMP satellite analysis of the lake basin. Water Resource Management 22 (7), 775–796, DOI:10.1007/s11269–007–9191–y.

Barletta, V., Sabadini, R., Bordoni, A., 2008. Isolating the PGR signal in the GRACE data: impact on mass balance estimates in Antarctica and Greenland. Geophysical Journal International 172 (1), 18–30, DOI:10.1111/j.1365–246X.2007.03630.x.

Baur, O., Kuhn, M., Featherstone, W., 2009. GRACE-derived ice-mass variations over Greenland by acocunting for leakage effects. Journal of Geophysical Research 114 (B06407), DOI:10.1029/2008JB006239.

Bettadpur, S., 2007. UTCSR Level-2 Processing Standards Document for Level-2 Product Release 0004. Gravity Recovery and Climate Experiment (GRACE) Rev 3.1, GRACE 327-742 (CSR-GR-03-03), Center for Space Research, The University of Texas at Austin.

Blais, J., Provins, D., 2002. Spherical harmonic analysis and synthesis for global multiresolution applications. Journal of Geodesy 76 (1), 29–35, DOI:10.1007/s001900100217.

Boy, J.-P., Chao, B., 2005. Precise evaluation of atmospheric loading effects on Earth's time-variable gravity field. Journal of Geophysical Research 110 (B08412), DOI:10.1029/2002JB002333.

Brown, N., Tregoning, P., 2010. Quantifying GRACE data contamination effects on hydrological analysis in the Murray-Darling Basin, southeast Australia. Australian Journal of Earth Sciences 57 (3), 329–335, DOI:10.1080/08120091003619241.

Bruinsma, S., Lemoine, J., Biancale, R., Valès, N., 2010. CNES/GRGS 10-day gravity field models (release 2) and their evaluation. Advances in Space Research 45 (4), 587–601, DOI:10.1016/j.asr.2009.10.012.

Chambers, D., Wahr, J., Nerem, R., 2004. Preliminary observations of

global ocean mass variations with GRACE. Geophysical Research Letters 31 (L13310), DOI:10.1029/2004GL020461.

Chen, J., Rodell, M., Wilson, C., Famiglietti, J., 2005. Low degree spherical harmonic influences on Gravity Recovery and Climate Experiment (GRACE) water storage estimates. Geophysical Research Letters 32 (L14405), DOI:10.1029/2005GL022964.

Chen, J., Wilson, C., Tapley, B., Yang, Z., Niu, G., 2009. 2005 drought event in the Amazon River basin as measured by GRACE and estimated by climate models. Journal of Geophysical Research 114 (B05404), DOI:10.1029/2008JB006056.

Crowley, J., Mitrovica, J., Bailey, R., Tamisea, M., Davis, J., 2006. Land water storage within the Congo Basin inferred from GRACE satellite gravity data. Geophysical Research Letters 33 (L19402), DOI:10.1029/2006GL027070.

Davie, T., 2008. Fundamentals of hydrology, 2nd Edition. Routledge, London.

Döll, P., Kaspar, F., Lehner, B., 2003. A global hydrological model for deriving water availability indicators: model tuning and validation. Journal of Hydrology 270 (1-2), 105–134, DOI:10.1016/S0022–1694(02)00283–4.

Ek, M., Mitchell, K., Lin, Y., Rogrs, E., Grunmann, P., Koren, V., Gayno, G., Tarp-

ley, J., 2003. Implementation of Noah land surface model advances in the National Centers for Environmental Prediction operational mesoscale Eta model. Journal of Geophysical Research 108 (D22), DOI: 10.1029/2002JD003296.

Ellett, K., Walker, J., Western, A., Rodell, M., 2006. A framework for assessing the potential of remote-sensed gravity to provide new insight on the hydrology of the Murry-Darling Basin. Australian Journal of Water Resources 10 (2), 125–138.

Fengler, M., Freeden, W., Kohlhaas, A., Michel, V., Peters, T., 2007. Wavelet modeling of regional and temporal variations of the earth's gravitational potential observed by GRACE. Journal of Geodesy 81 (1), 5–15, DOI:10.1007/s00190–006–0040–1.

Güntner, A., Stuck, J., Döll, P., Schulze, K., Merz, B., 2007. A global analysis of temporal and spatial variations in continental water storage. Water Resources Research 43 (W05416), DOI:10.1029/2006WR005247.

Han, S.-C., Shum, C., Braum, A., 2005. High-resolution continental water storage recovery from low-low satellite-to-satellite tracking. Journal of Geodynamics 39 (1), 11–28, DOI:10.1016/j.jog.2004.08.002.

Huffman, G., Adler, R., Bolvin, D., Gu, G., Nelkin, E., Bowman, K.,

Hong, Y., Stocker, E., Wolff, D., 2007. The TRMM Multisatellite Precipitation Analysis (TMPA): Quasi-global, multiyear, combined-sensor precipitation estimates at fine scales. Journal of Hydrometeorology 8 (1), 38–55, DOI:10.1175/JHM560.1.

Klosko, S., Rowlands, D., Luthcke, S., Lemoine, F., Chinn, D., Rodell, M., 2009. Evaluation and validation of mascon recovery using GRACE KBRR data with independent mass flux estimates in the Mississippi Basin. Journal of Geodesy 83 (9), 817–827, DOI:10.1007/s00190–009–0301–x.

Kummerow, C., Barnes, W., Kozu, T., Shiue, J., Simpson, J., 1998. The Tropical Rainfall Measuring Mission (TRMM) sensor package. Journal of Atmospheric and Oceanic Technology 15 (3), 809–817, DOI:10.1175/1520–0426(1998)015<0809:TTRMMT>2.0.CO;2.

Kummerow, C., Simpson, J., Thiele, O., Barnes, W., Chang, A., Stocker, E., Adler, R., Hou, A., Kakar, R., Wntz, F., Aschroft, P., Kozu, T., Hing, Y., Okamoto, K., Iguchi, T., Kuroiwa, H., Im, E., Haddad, Z., Huffman, G., Ferrier, B., Olson, W., Zipser, E., Smith, E., Wilheit, T., North, G., Krishnamurti, T., Nakamura, K., 2000. The status of the Tropical Rainfall Measuring Mission (TRMM) af-

ter two years in orbit. Journal of Applied Meteorology 39 (12), 1965–1982, DOI:10.1175/1520–0450(2001)040<1965:TSOTTR>2.0.CO;2.

Leblanc, M., Tregoning, P., Ramillien, G., Tweed, S., Fakes, A., 2009. Basin-scale, integrated observations of the early 21st century multiyear drought in southeast Australia. Water Resources Research 45 (W04408), DOI:10.1029/2008WR007333.

Lemoine, F., Luthcke, S., Rowlands, D., Chinn, D., Klosko, S., Cox, C., 2007a. The use of mascons to resolve time-variable gravity from GRACE. In: Tregoning, P., Rizos, C. (Eds.), Dynamic Planet. Springer, Berlin, pp. 231–236.

Lemoine, J.-M., Bruinsma, S., Loyer, S., Biancale, R., Marty, J.-C., Perosanz, F., Balmino, G., 2007b. Temporal gravity field models inferred from GRACE data. Advances in Space Research 39 (10), 1620–1629, DOI:10.1016/j.asr.2007.03.062.

Luthcke, S., Rowlands, D., Lemoine, F., Klosko, S., Chinn, D., McCarthy, J., 2006. Monthly spherical harmonic gravity field solutions determined from GRACE inter-satellite range-rate data alone. Geophysical Research Letters 33 (L02402), DOI:10.1029/2005GL024846.

Melachroinoa, S., lemoine, J.-M., Tregoning, P., Biancale, R., 2009. Quantify-

ing FES2004 S_2 tidal model from mulitple space-geodesy techniques, GPS and GRACE, over North West Australia. Journal of Geodesy 83 (10), 915–923, DOI: 10.1007/s00190–009–0309–2.

Milani, A., Nobili, A., Farinella, P., 1987. Non-gravitational perturbations and satellite geodesy. Adam Hilger Ltd., Bristol.

Montgomery, D., Peck, E., 1992. Introduction to linear regression analysis, 2nd Edition. John Wiley & Sons Inc., New York.

Muller, P., Sjogren, W., 1968. MASCONS - lunar mass concentrations. Science 161 (3842), 680–684, DOI:10.1126/science.161.3842.680.

Nicholls, N., 2004. The changing nature of Australian droughts. Climatic Change 63 (3), 323–336, DOI:10.1023/B:CLIM.0000018515.46344.6d.

Nicholls, N., 2006. Detecting and attributing Australian climate change: a review. Australian Meteorological Magazine 55 (3), 199–211.

Preisendorfer, R., 1988. Principal component analysis in meteorology and oceanography. Elsevier, Amsterdam, New York.

Ramillien, G., Cazenave, A., Brunau, O., 2004. Global time variations of hydro-

logical signals from GRACE satellite gravimetry. Geophysical Journal International 158 (3), 813–826, DOI:10.1111/j.1365–246X.2004.02328.x.

Rieser, D., Kuhn, M., Pail, R., Anjasmara, I., Awange, J., 2010. Relation between GRACE-derived surface mass variations and precipitation over Australia. Australian Journal of Earth Science 57 (7), 887–900, DOI: 10.1080/08120099.2010.512645.

Rodell, M., Famiglietti, J., 1999. Detectability of variations in continental water storage from satellite observations of the time dependent gravity field. Water Resources Research 35 (9), 2705–2723, DOI:10.1029/1999WR900141.

Rodell, M., Houser, P., Jambor, U., Gottschalck, J., Mitchell, K., Meng, C.-J., Arsenault, K., Cosgrove, B., Radakovich, J., Bosilovich, M., Entin, J., Walker, J., Lohmann, D., Toll, D., 2004. The Global Land Data Assimilation System. Bulletin of the American Meteorological Society 85 (3), 381–394, DOI:10.1175/BAMS–85–3–381.

Rowlands, D., Luthcke, S., Klosko, F., Chinn, D., McCarthy, J., Cox, C., Anderson, O., 2005. Resolving mass flux at high spatial and temporal resolution using GRACE intersatellite measurements. Geophysical Research Letters 32 (L04310), DOI:10.1029/2004GL021908.

Rowlands, D., Luthcke, S., McCarthy, J., Kosko, S., Chinn, D., Lemoine, F., Boy, J.-P., Sabaka, T., 2010. Global mass flux solutions from GRACE: A comparison of parameter estiation strategies - Mass concentration versus Stokes coefficients. Journal of Geophysical Research 115 (B01403), DOI:10.1029/2009JB006546.

Solomon, S., Qin, D., Manning, M., Chen, Z., Marquis, M., Averyt, K., M., T., Miller, H. (Eds.), 2007. Contribution of Working Group 1 to the Fourth Assessment Report of the Intergovernmental Panel on Climate Change. Cambridge University Press.

Swenson, S., Wahr, J., 2002. Estimated effects of the vertical structure of atmospheric mass on the time-variable geoid. Journal of Geophysical Research 107 (B9), DOI:10.1029/2000JB000024.

Swenson, S., Wahr, J., 2006. Post-processing removal of correlated errors in GRACE data. Geophysical Research Letters 33 (L08402), DOI:10.1029/2005GL025285.

Swenson, S., Wahr, J., Milly, P., 2003. Estimated accuracies of regional water storage variations inferred from the Gravity Recovery and Climate Experiment (GRACE). Water Resources Research 39 (8), DOI:10.1029/2002WR001808.

Syed, T., Famiglietti, J., Chen, J., Rodell, M., Seneviratne, S., Viterbo, P., Wilson, C., 2005. Total basin discharge for the Amazon and Mississippi River basins from GRACE and a land-atmosphere water balance. Geophysical Research Letters 32 (L24404), DOI:10.129/2005GL024851.

Syed, T., Famiglietti, J., Rodell, M., Chen, J., Wilson, C., 2008. Total basin discharge for the Amazon and Mississippi River basins from GRACE and a land-atmosphere water balance. Water Resources Research 44 (W02433), DOI:10.129/2006WR005779.

Tapley, B., Bettadpur, S., Ries, J., Thompson, P., Watkins, M., 2004a. GRACE measurements of mass variability in the Earth system. Science 305, 503–505, DOI:10.1126/science.1099192.

Tapley, B., Bettadpur, S., Watkins, M., Reigber, C., 2004b. The gravity recovery and climate experiment: Mission overview and early results. Geophysical Research Letters 31 (L09607), DOI:10.1029/2004GL019920.

Tapley, B., Ries, J., Bettadpur, S., Chambers, D., Cheng, M., Condi, F., Gunter, B., Kang, Z., Nagel, P., Pastpr, R., Pekker, T. Poole, S., Wang, F., 2005. GGM02 - An improved Earth graivty field model from GRACE. Journal of Geodesy 79 (8), 467–478, DOI: 10.1007/s00190–005–0480–z.

Tiwari, V., Wahr, J., Swenson, S., 2009. Dwindling groundwater resources in northern India, from satellite gravity observations. Geophysical Research Letters 36 (L18401), DOI:10.1029/2009GL039401.

Tregoning, P., Ramillien, G., McQueen, H., Zwartz, D., 2009. Glacial isostatic adjustment and nonstationary signals observed by GRACE. Journal of Geophysical Research 114 (B06406), DOI:10.1029/2008JB006161.

Ummenhofer, C., England, M., McIntosh, P., Meyers, G., Pook, M., Risbey, J., Gupta, A., Taschetto, A., 2009. What causes southeast Australia's worst droughts? Geophysical Research Letters 36 (L04706), DOI:10.1029/2008GL036801.

Velicogna, I., 2009. Increasing rates of ice mass loss from the Greenland and Antarctic ice sheets revealed by GRACE. Geophysical Research Letters 36 (L19503), DOI:10.1029/2009GL040222.

Wahr, J., Jayne, S., Bryan, F., 2002. A method of inferring changes in deep ocean currents from satellite measurements of time-variable gravity. Journal of Geophysical Research 107 (C12), DOI:10.1029/2002JC001274.

Wahr, J., Molenaar, M., Bryan, F., 1998. Time variability of the Earth's gravity field: Hydrological and oceanic effects and their possible detection us-

ing GRACE. Journal of Geophysical Research 103 (B12), 30205–30229, DOI:10.1029/98JB02844.

Werth, S., Güntner, A., Petrovic, S., Schmidt, R., 2009. Integration of GRACE mass variations into a global hydrological model. Earth and Planetary Science Letters 27 (1-2), 166–173, DOI:10.1016/j.epsl.2008.10.021.

Wessel, P., Smith, W., 1998. New, improved version of Generic Mapping Tools released. EOS Transactions of the American Geophysical Union 79 (47), 579, DOI:10.1029/98EO00426.

Table 1: The cross-correlations (Eqn. 4) between the different datasets for the linear and annual amplitude and annual phase terms (Figure 4). White cells are for the linear term, light grey cells are for the annual amplitude/phase terms.

	mascon	CNES/GRGS	CSR	TRMM	GLDAS	WGHM
mascon		0.70	0.68	0.36	0.50	0.31
CNES/GRGS	0.88/0.89		0.72	0.26	0.55	0.29
CSR	0.85/0.83	0.95/0.75		0.19	0.58	0.33
TRMM	0.79/0.74	0.94/0.70	0.93/0.75		0.32	0.41
GLDAS	0.81/0.83	0.94/0.79	0.90/0.82	0.97/0.67		0.48
WGHM	0.76/0.70	0.86/0.69	0.81/0.76	0.88/0.69	0.91/0.72	

Table 2: The cross-correlations (Eqn. 4) between the different datasets for the sectors that the MDB is divided into (Figure 5).

Combination	Sector A	Sector B	Sector C	Sector BC
mascon - CNES/GRGS	0.70	0.74	0.78	0.79
mascon - CSR	0.75	0.78	0.82	0.81
CSR - CNES	0.83	0.88	0.94	0.93
mascon - TRMM	0.18	0.61	0.70	0.66
CNES/GRGS - TRMM	0.55	0.81	0.72	0.80
CSR - TRMM	0.27	0.71	0.76	0.75
mascon - GLDAS	0.43	0.42	0.63	0.50
CNES/GRGS - GLDAS	0.81	0.70	0.78	0.76
CSR - GLDAS	0.65	0.66	0.80	0.74
mascon - WGHM	0.43	0.69	0.61	0.67
CNES/GRGS - WGHM	0.49	0.81	0.67	0.79
CSR - WGHM	0.35	0.74	0.73	0.75
TRMM - GLDAS	0.56	0.75	0.82	0.80
TRMM - WGHM	0.54	0.81	0.81	0.83
GLDAS - WGHM	0.70	0.80	0.86	0.87
River gauge - mascon		0.39	0.36	0.30
River gauge - CNES/GRGS		0.68	0.41	0.53
River gauge - CSR		0.51	0.42	0.40

FIGURE 1

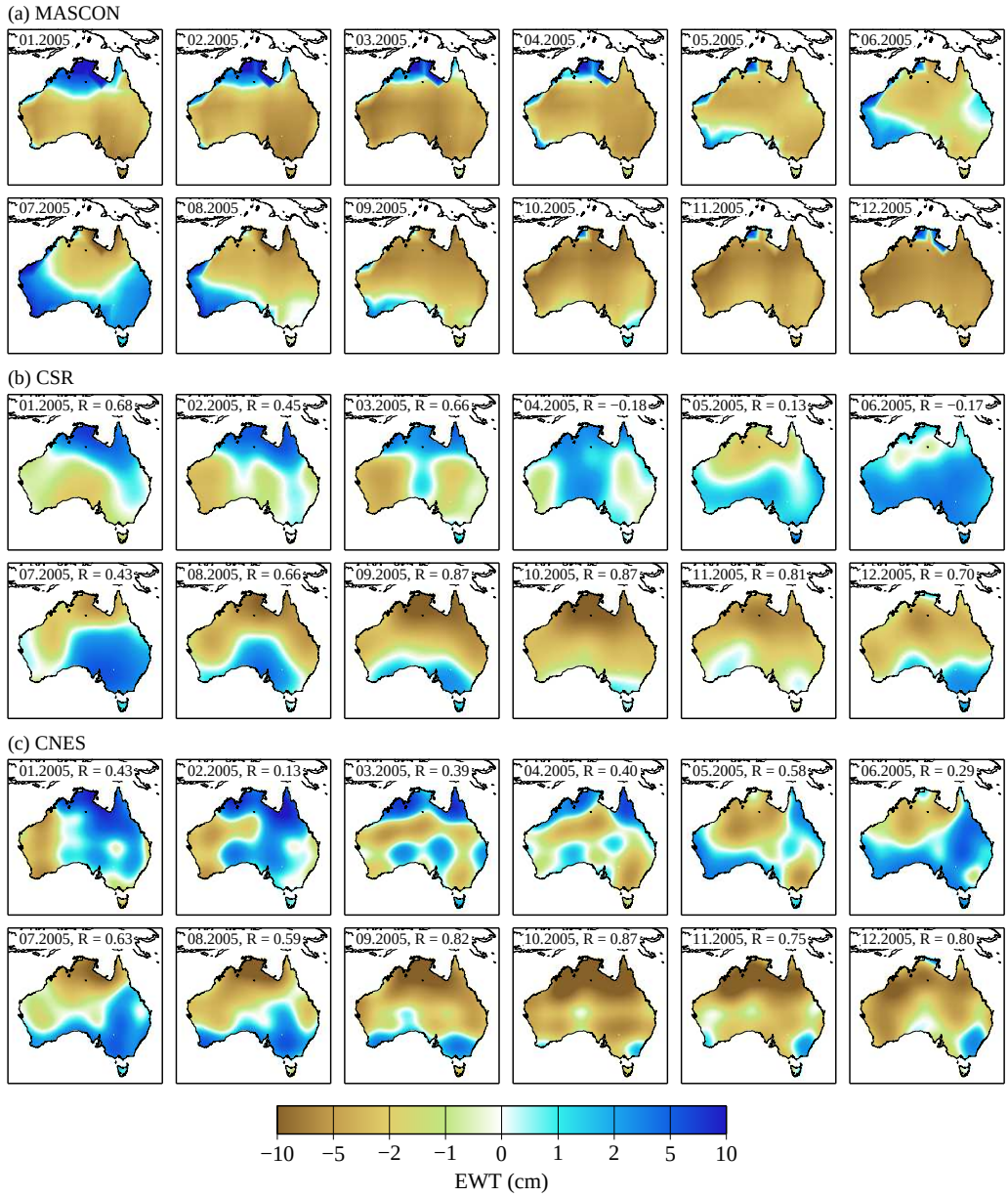

Figure 1: GRACE solutions for 2005: (a) mascon solutions (average of three 10-day solutions), (b) CSR (RL04 solutions), and (c) CNES/GRGS (average of three 10-day RL02 solutions). All are expressed as equivalent water thickness (EWT, cm) (Lambert conformal conic projection). The R values in (b) and (c) represent the cross correlation between each CSR or CNES/GRGS month and its mascon equivalent (Eqn. 4).

FIGURE 2

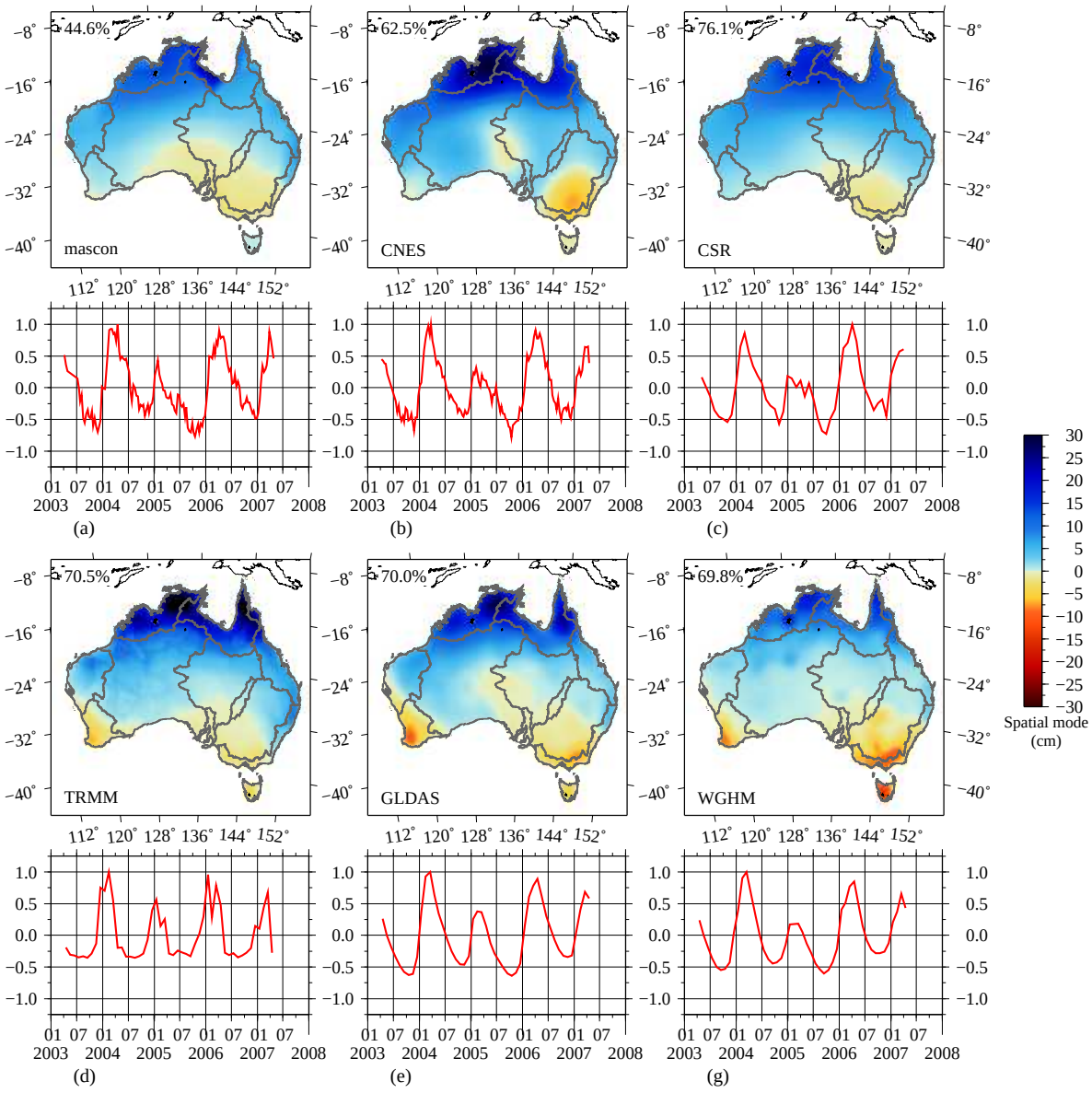

Figure 2: Results of the PCA applied to the whole of Australia for the 1st mode. (a) mascon, (b) CNES/GRGS, (c) CSR, (d) TRMM, (e) GLDAS and (f) WGHM. Australia's drainage divisions (from the Australian Bureau of Meteorology, see the Acknowledgements) are marked by the grey boundaries (Lambert conformal conic projection).

FIGURE 3

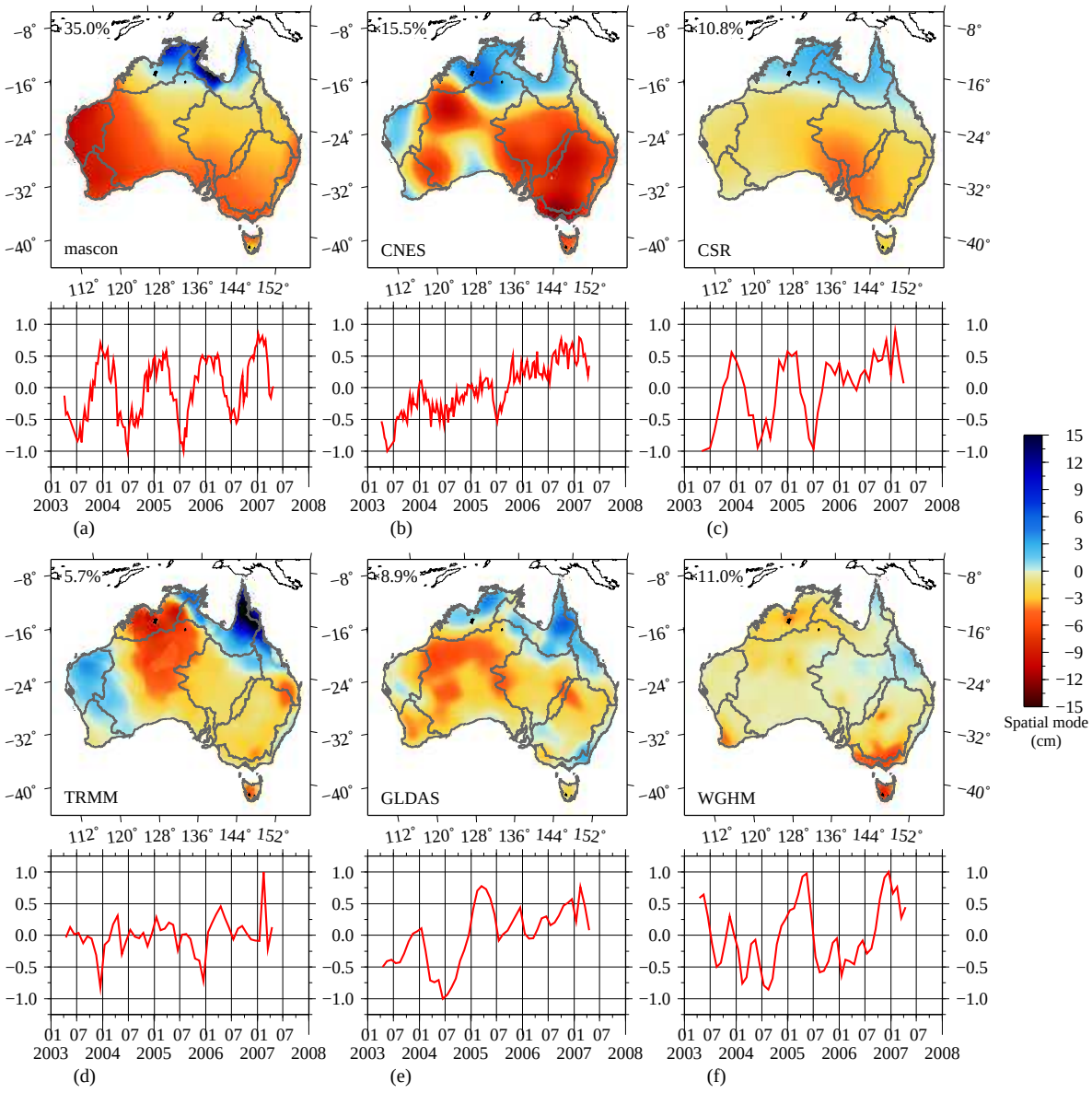

Figure 3: As in Figure 2 but for mode 2.

FIGURE 4

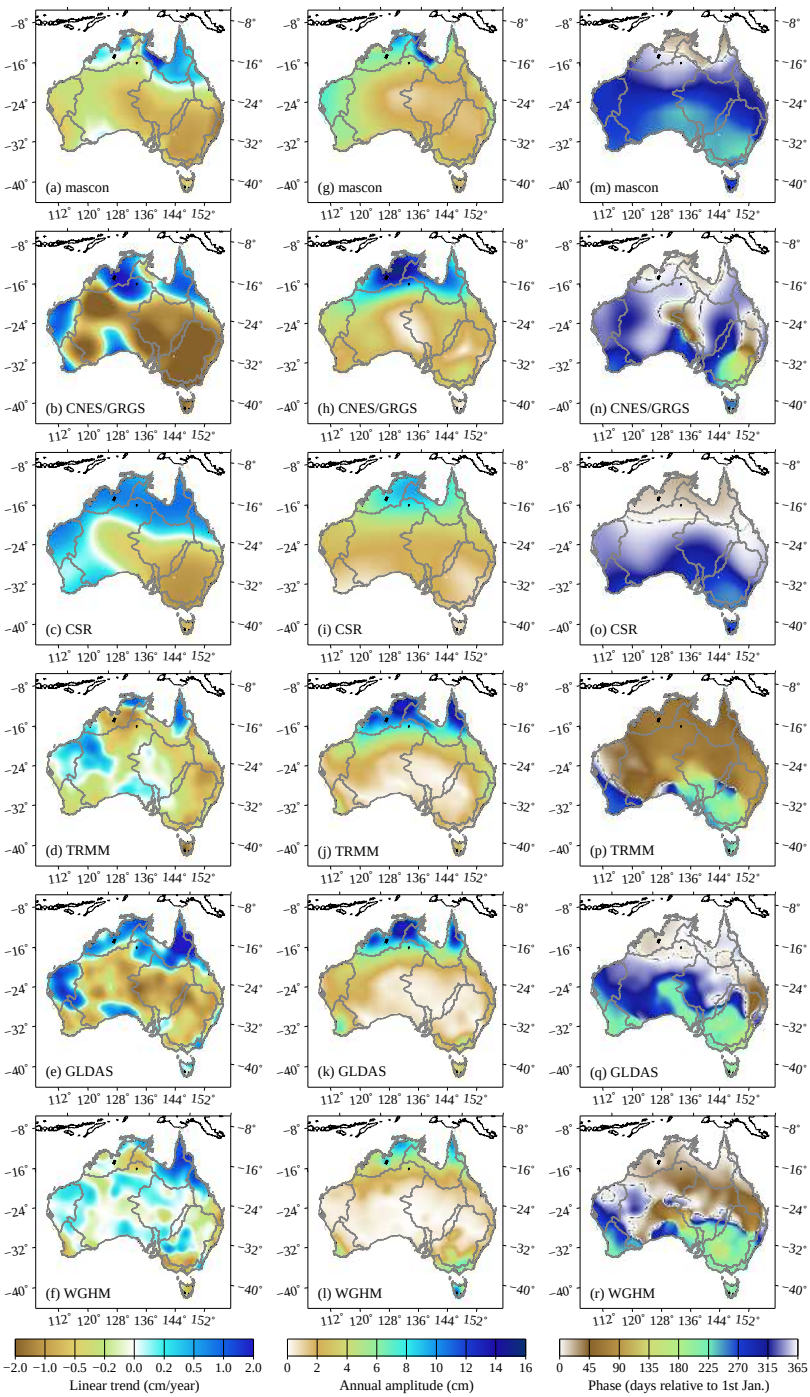

Figure 4: The linear trend (a-f), annual amplitude (g-l) and phase (m-r) (Eqn. 4). (a,g,m) mascon, (b,h,n) CNES/GRGS, (c,i,o) CSR, (d,j,p) TRMM, (e,k,q) GLDAS and (f,l,r) WGHM. Australia's drainage divisions (from the Australian Bureau of Meteorology, see the Acknowledgements) are marked by the grey boundaries (Lambert conformal conic projection).

FIGURE 5

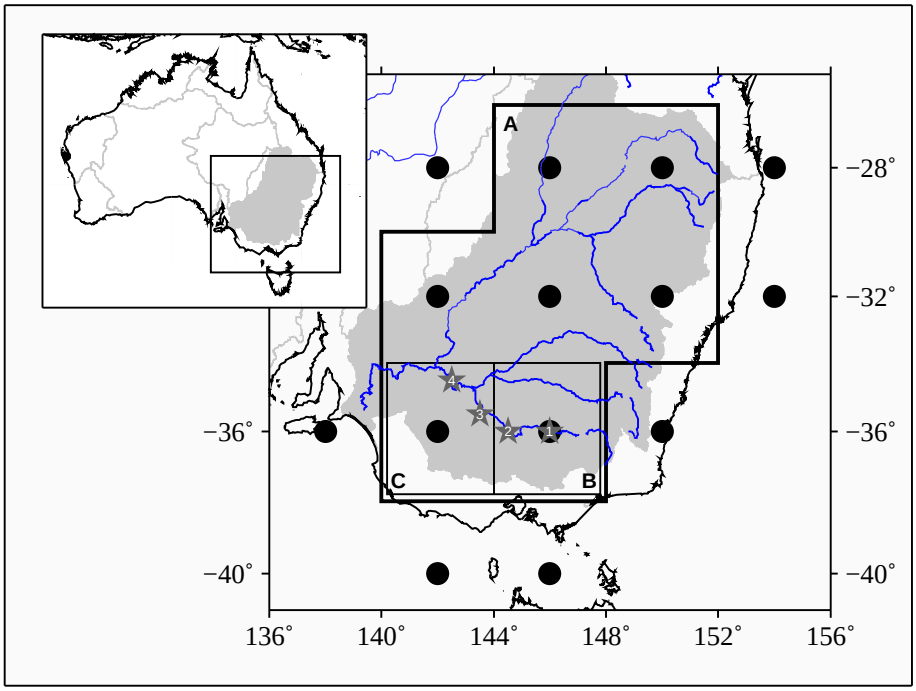

Figure 5: Location map of the Murray-Darling Basin (MDB). The grey shading marks the basin's extent, with Australia's other river basins also outlined in grey. Black filled circles are the centres of the mascon grid cells provided by GSFC ($4° \times 4°$ grid). The thick black-bounded area (A) covers most of the MDB, while the finer black-bounded areas (B and C) are examined with respect to ground-truth data in the form of river-gauge data (numbered stars). The river-gauges are at Yarrawonga (1), Swan Hill (2), Euston (3) and Torrumbarry (4).

FIGURE 6

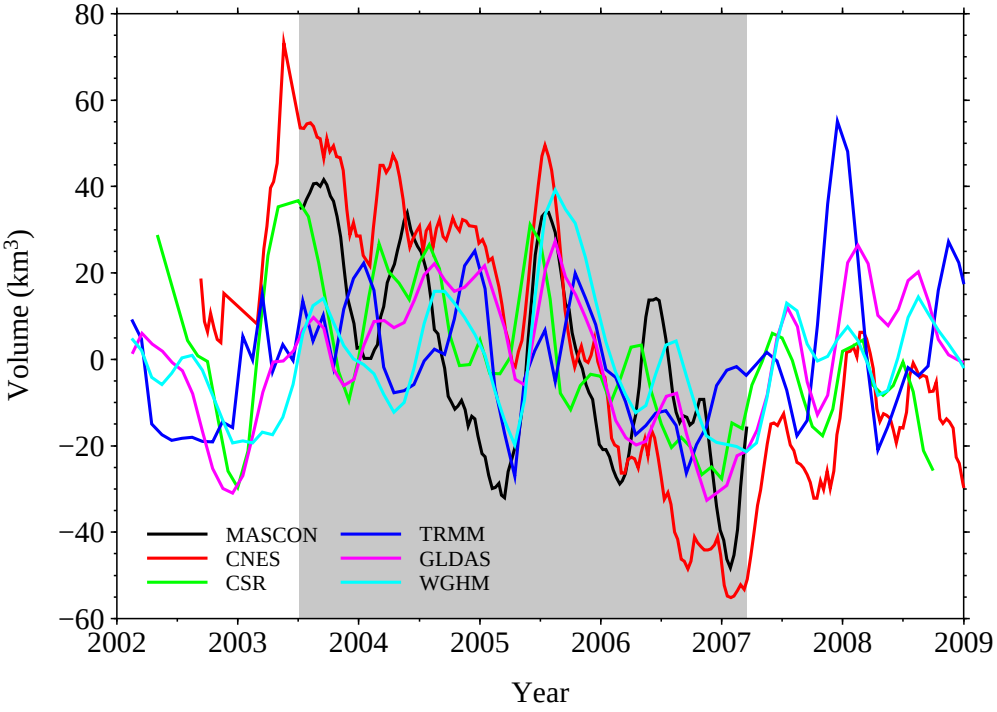

Figure 6: The change in equivalent water volume (EWV) over the MDB, as outlined by sector A in Figure 5 for the datasets used in this work. A three-month moving average has been applied to each time-series. The gray shading marks the time span over which the mascon solutions are available. Cross-correlations between pairs of datasets are listed in Table 2.

FIGURE 7

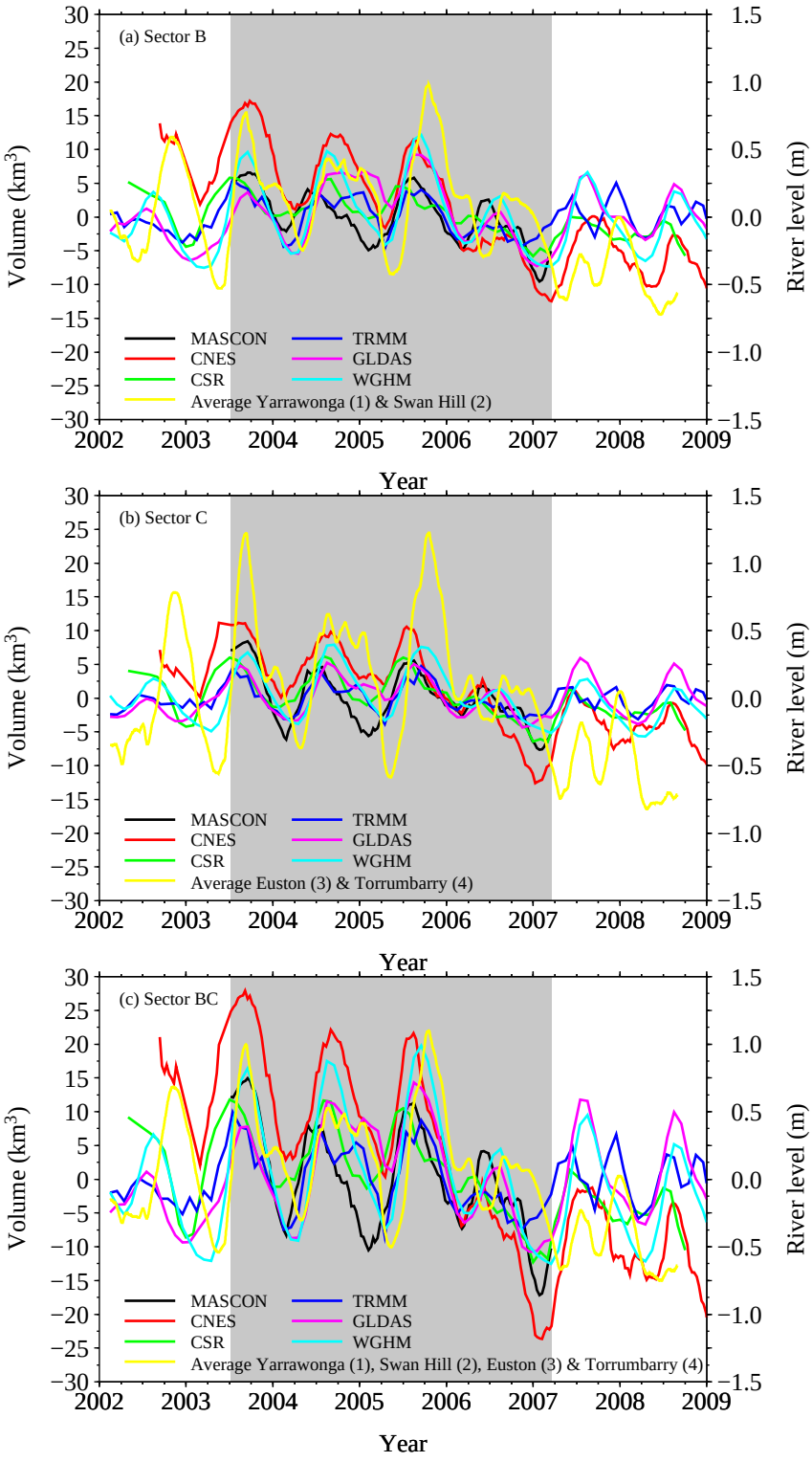

Figure 7: As in Figure 6, but for the smaller sectors outlined in Figure 5: (a) sector B, (b) sector C, (c) sectors B and C (BC). Also marked are river-gauge time-series. All time-series are smoothed with a three month moving average. Cross-correlations between pairs of datasets are listed in Table 2.